Analyzing Chaotic Behavior in a Belousov−Zhabotinskyi Reaction by Using a Global Vector Field Reconstruction

C. Letellier,* J. Maquet, H. Labro, L. Le Sceller, and G. Gouesbet

Université et INSA de Rouen−CORIA UMR 6614, Place Emile Blondel, 76131 Mont Saint-Aignan Cedex, France

F. Argoul and A. Arnéodo

Centre de Recherche Paul Pascal, Avenue Schweitzer, 33600 Pessac, France

Received: May 12, 1998; In Final Form: September 28, 1998

The Belousov−Zhabotinskyi reaction is governed by very complex chemical kinetics involving at least 20 species. Nevertheless, there are many results that suggest that such a reaction could be described by a 3D model. For instance, in the special case when the asymptotic behavior is close to a homoclinic orbit, a 3D normal-form model has been previously proposed. Rather than deriving such a model, which requiring prior knowledge about the dynamics, a 3D model is here obtained by using a global vector field reconstruction technique starting from the measured time dependence of [CeIV]. This reconstructed model is hereafter validated by comparing the topological properties of the associated attractor to the ones directly reconstructed from the time series by using derivative coordinates. Indeed, the template characterizing the reconstructed model is compatible with the one extracted from the data. Nevertheless, it is found to be not compatible with the template associated with the normal-form model, which does not generate trajectories close enough to the experimental ones. Consequently, the topological properties of the underlying dynamics are not well captured by the normal-form model.

1. Introduction

Experimental observations of oscillations in chemically reacting systems date back at least to the 1950s, but the actual growth of interest in the subject occurred with the paper by Zhabotinskii in 1964.[1] First, the most interesting phenomena that occur in bromate ion driven chemical oscillations whose mechanism was elucidated in 1972 by Field et al[2] have played a critical role in the development of solution-phase oscillating chemical reactions. The discovery by Belousov[3] of the cerium ion catalyzed oxidation and bromination of citric acid by BrO_3^-, marked the beginning of the modern era of research in the topic. The work by Belousov was extended by Zhabotinskii.[1] The systems based on either the cerous/ceric or on the ferroin/ferric redox couples with malonic acid are of particular interest and received the name of these investigators. Second, the observations and investigations of chaotic behaviors in chemical reactions[4] lead to the conclusion that nonperiodic behaviors genuinely arise from the nonlinear nature of deterministic systems rather than from a noisy behavior produced by random driving forces.

The mechanism of the Belousov−Zhabotinskyi (BZ) reaction elucidated by Field et al[2] and further elaborated[5] involves more than 20 species and is slaved however to a few species. Hence, it has been possible to develop a reduced model given by reactions with nine intermediate species including an oxidized derivative (R) of malonic acid (MA), an inert organic product (P), and bromomalonic acid (BrMA). The concentrations of both bromate and cerous ions are assumed to be constant in the reactor, and only the input flow of Br is taken into account in the calculations.[6] This model was shown to be sufficient to qualitatively reproduce the main features of the BZ-reaction.[7] Explicitly, this model reads

$$BrO_3^- + Br^- + 2H^+ \rightarrow HBrO_2 + HOBr \quad \text{(R1)}$$

$$HBrO_2 + Br^- + H^+ \rightarrow 2HOBr \quad \text{(R2)}$$

$$HOBr + Br^- + H^+ \rightarrow Br_2 + H_2O \quad \text{(R3)}$$

$$BrO_3^- + HBrO_2 + H^+ \leftrightarrow 2BrO_2 + H_2O \quad \text{(R4)}$$

$$2HBrO_2 \rightarrow BrO_3^- + HOBr + H^+ \quad \text{(R5)}$$

$$BrO_2 + Ce^{3+} + H^+ \rightarrow HBrO_2 + Ce^{4+} \quad \text{(R6)}$$

$$HOBr + MA \rightarrow BrMA + H_2O \quad \text{(R7)}$$

$$BrMA + Ce^{4+} \rightarrow Br^- + R + Ce^{3+} + H^+ \quad \text{(R8)}$$

$$R + Ce^{4+} \rightarrow Ce^{3+} + P \quad \text{(R9)}$$

Reactions R1−R9 translate into a system of seven ordinary differential equations, which when simulated on a computer, yields a bifurcation diagram similar to the one experimentally observed.[7] The model (R1−R9), which may be reduced to a seven-variable model, shows that chaos indeed occurs in the neighborhood of the transitions between different periodic states.[6,8] All the strange attractors that have been studied, obtained from both simulations and experiments, can be embedded in a tridimensional space.[6−11]

Moreover, an analysis in normal forms, which leads to the simplest nonlinear equations describing bifurcations, demon-

10.1021/jp982219u CCC: $15.00
Published on Web 11/21/1998

strated that a system of coupled differential equations with only three variables can describe most of the dynamics found in the BZ reaction, including quasiperiodicity and large- and small-scale chaos.[8] This model will be called the normal-form model (NF model) in this paper. Thus, a reduction of the original Field−Körös−Noyes scheme involving 20 species to a three-variable skeletal mechanism appears to be justified. The three-variable NF model reproduces the interaction between a Hopf bifurcation and a homoclinic bifurcation as experimentally observed.[7] Nevertheless, by a simple visual inspection of phase portraits, it appears that such a low-dimensional model does not capture the dynamics of the experiments with sufficient accuracy. The aim of this paper is therefore to provide a three-variable model for the BZ reaction that reproduces in a better way the experimental data. This new model will be obtained by using a global vector field reconstruction technique that extracts, rather automatically, a set of ordinary differential equations from the data. Also, by using a topological characterization, we will show that the model allows one to investigate the fine structure of the dynamics, which is not easily available from the experimental data.

This work provides a new contribution to the important problem of the modeling and topological analysis of data. Such an analysis has been previously achieved in the case of a copper electrodissolution, where the dynamics was found to be governed by a horseshoe dynamics.[12] Brown et al[13] also proposed an analysis using a similar technique on data generated by string experiments, a BZ reaction, and an electronic circuit, which are also governed by a horseshoe dynamics, except for the electronic circuit whose topological properties exhibit a more complicated dynamics as discussed in ref 14. In the present case, the asymptotic behavior is close to a homoclinic orbit, which induces a very complex attractor. Such a dynamical behavior is especially difficult to analyze. In particular, it is not so easy to obtain a reconstructed model compared with simpler cases characterized by a horseshoe dynamics since oscillations with two different time scales are now involved in the process.

The paper is organized as follows. Section 2 is devoted to the analysis of experimental data. Basic concepts of topological characterization are also introduced. A reconstructed model, obtained using a global vector field reconstruction technique, is found to be in a good agreement with the dynamics underlying the low-amplitude oscillations (Section 3). In section 4, the NF model is rejected since its topological characterization provides a template not compatible with the one extracted from the data. Section 5 is a conclusion.

2. Analysis of the Experimental Data

A. Experiments. The Belousov−Zhabotinskyi reaction is performed in an open, continuously stirred tank reactor (27 mL volume) fed by three feed lines:[18]

first line: $[NaBrO_3] = 7.5 \times 10^{-3}$ mol L^{-1}; $[H_2SO_4] = 1.5$ N

second line: $[CH_2(COOH)_2] = 0.15$ mol L^{-1}; $[H_2SO_4] = 1.5$ N

third line: $[Ce_2(SO_4)_3] = 5 \times 10^{-4}$ mol L^{-1}; $[H_2SO_4] = 1.5$ N

The three fluxes are maintained nearly equal by using a peristaltic pump. The flow rate through the reactor (φ) plays the role of the control parameter; for the present analysis, it is fixed to 0.130 mL mn^{-1}. The dynamics is monitored by measuring the absorbance of the solution at 360 nm. The stirring rate is 600 rpm, while the temperature is regulated to 41 °C. The time dependence of [CeIV] is recorded, and a part of the time series is displayed in Figure 1. The time series is recorded during a 20 h experiment. Beyond this time, experimental drifts are unavoidable. To prevent our analysis from being spoiled by this drift, the linear drift whose slope is found to be equal to 0.000 114 5 is removed before data processing. The noise contamination is also partially removed by using a Fourier transform. Of course, it remains possible that drifts on shorter time scales affect the dynamics, but as it is not easily identifiable, such short drifts are considered as a part of the dynamics studied.

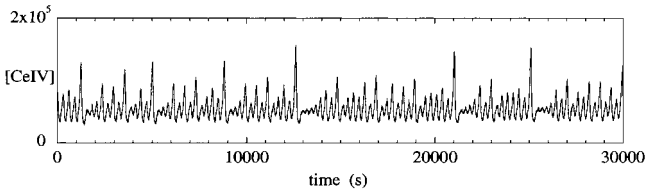

Figure 1. Time evolution of [CeIV] in the case of homoclinic chaos evidenced in the BZ experiments.

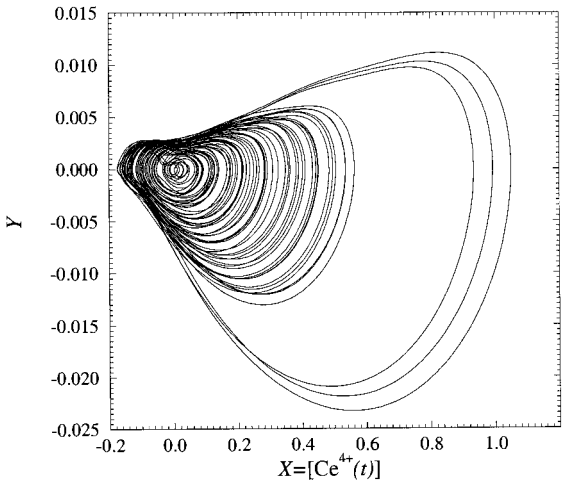

Figure 2. Phase space projection obtained by using derivative coordinates from the experimental time series.

B. Template Extraction from the Data. As discussed in the Introduction, many works point to the fact that the dynamics of the BZ reaction can be embedded in a tridimensional space, implying that a 3D model should be sufficient to accurately describe the dynamical behavior of this chemical reaction. Following a theorem by Takens,[15] it is possible to obtain a reconstruction of the phase space starting from a scalar time series by using time delay coordinates or derivative coordinates. Principal components[16] may also be equivalently used since Gibson et al[17] demonstrated that these three kinds of coordinates are equivalent. In the present case, we prefer to use the derivative coordinates, which will then later allow a direct comparison with the phase portrait obtained by integrating a model extracted from the experimental data by using a global vector field reconstruction technique (see section 3). Consequently, a phase space spanned by the time series $X(t) = [Ce^{4+}(t)]$ and its two first time derivatives, $Y = \dot{X}$ and $Z = \ddot{X}$, is used to investigate the topological properties of the underlying dynamics. A plane projection of the reconstructed phase space is displayed in Figure 2.

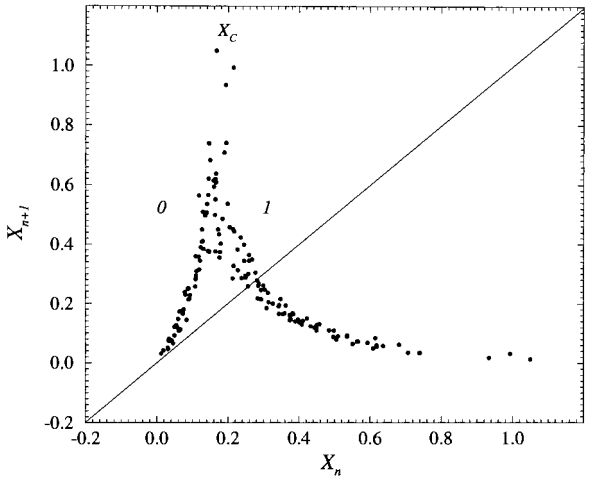

Figure 3. First-return map computed in the reconstructed phase space from the experimental time series.

The trajectory recurrently returns to the vicinity of the saddle focus and close enough to it in such a way that the chaotic attractor does not contain any significant central hole, in contrast to the chaotic behavior studied by Mindlin et al[11] or by Brown et al.[13] Indeed, a homoclinic reinjection process to the neighborhood of an underlying saddle focus has been reported.[18]

A first-return map to a Poincaré section is afterward computed. As a result of the lack of a significant hole in the middle of the attractor, we cannot claim that this return map is very accurate. Furthermore, despite the large recording time during the experiments, only 266 points are found in the Poincaré section with only a few of them with large amplitude oscillations. Nevertheless, two (not well visited) monotonic branches may be exhibited (Figure 3). Each monotonic branch is labeled by an integer allowing one to encode periodic orbits by symbolic sequences, namely 0 for the increasing branch and 1 for the decreasing branch.

The extraction and coding of periodic orbits is a step in the topological characterization of the attractor. Periodic orbits are extracted by Newton−Raphson iterations scheme to identify close returns. Again, as a result of the lack of a significant hole in the middle of the attractor, this step is not as easy as usual. Furthermore, a partially inadequate embedding is unfortunately obtained from the time series since many spurious and ambiguous crossings occur in the neighborhood of the fixed point where the noise contamination degrades the observability of the dynamical structure. It therefore appears difficult to accurately count oriented crossings required for estimating linking numbers between pairs of periodic orbits, as required for a refined topological characterization.[19,20] In addition, the trajectory does not visit the monotonic branches of the first-return map well enough (Figure 3), leading to difficulties in extracting the population of periodic orbits in a complete reliable way. Notwithstanding these problems, we have been nevertheless able to produce the results displayed in Table 1, to be again discussed later.

It is well-known that a chaotic attractor is structured around a skeleton of periodic orbits. In particular, the idea has arisen that an attractor can be described by its population of periodic orbits, their related symbolic dynamics, and their linking numbers.[21] In three-dimensional cases, periodic orbits may be viewed as knots,[19] and consequently, they are robust with respect to smooth parameter changes as far as they are not implied in a bifurcation. Such properties allow the definition of topological invariants under isotopy (continuous deformation).

TABLE 1: Population of Periodic Orbits Extracted from the Experimental Data and Their Linking Number[a]

	(1)	(10)	(1011)	(10111)	(10110)
(10)	−1				
(101)	−1	[−2]			
(1011)	[−2]	[−3]	[−4]		
(10111)	−2	−4	[−5]	[−8]	
(10110)	[−2]	−5	[−5]	[−8]	[−10]

[a] Values in square brackets have been obtained using the corrections described in the text.

The topological approach is based on the relative organization of periodic orbits previously discussed. Once the periodic orbits are extracted, one may then define a partition of the attractor relying on the critical points of the first-return map (Figure 3). In the case of our experimental data, periodic orbits are encoded by strings of symbols σ_n defined as

$$\sigma_n = \begin{cases} 0 & \text{if } X_n < X_C \\ 1 & \text{if } X_n > X_C \end{cases} \tag{1}$$

where X_n is the coordinate of the nth intersection of the chaotic trajectory with a Poincaré section and $X_C \approx 0.12$ defines the critical point exhibited on the first-return map (Figure 3). Afterward, we have to compute linking numbers for pairs of extracted periodic orbits. This ambient isotopy invariant is defined as follows.

Let α and β be two knots defining a link L in R^3. Let σ denote the set of crossings of α with β. Then the linking number reads as

$$\mathrm{lk}(\alpha,\beta) = \frac{1}{2}\sum_{p\in\sigma} \epsilon(p) \tag{2}$$

where ϵ is the sign of each crossing p with the usual convention; that is

The linking number lk(α,β) of two periodic orbits α and β is therefore the half of the algebraic sum of all crossings between α and β (ignoring self-crossings).

From experimental data, the linking numbers are counted on plane regular projections of orbit pairs by using the third coordinate to define the sign of the crossings. For instance, the case of orbits 1 and 10 is displayed in Figure 4. This example is very simple, but we may encounter more ambiguous cases where oriented crossings are not so easily computed. Difficulties arise when segments of two different periodic orbits are close to tangency. In this case, spurious crossings may appear as displayed in Figure 5. Such spurious crossings may come from the smoothing applied on the data, since it is known that Fourier transform may imply additional oscillations. Without this filtering however, the situation would be worse due to spurious crossings generated by noise. Consequently, we choose to remove by hand the spurious crossings. Two cases of removal are observed as displayed in Figure 6.

Crossings are considered as spurious if they correspond to high-frequency oscillations in the signal, i.e., frequencies large with respect to the frequency associated with the pseudoperiod. In other terms, crossings between two strands may be considered as spurious when the distance between the crossings is smaller. In the case of Figure 6a, crossings are not taken into account

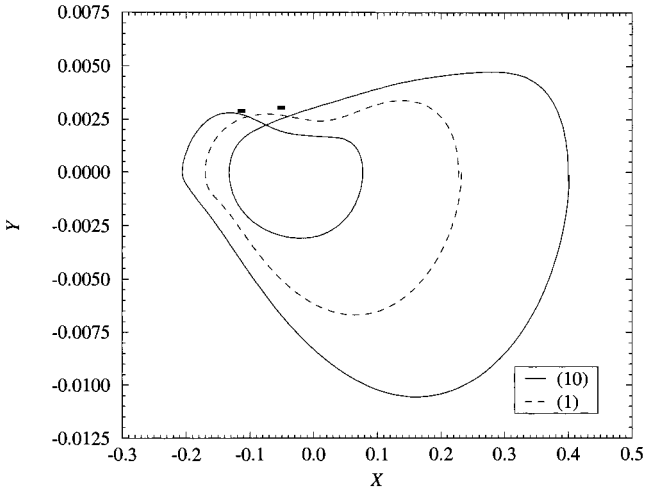

Figure 4. Plane projection of a couple of periodic orbits encoded by (1) and (10), respectively. The associated linking number is equal to the half sum of the oriented crossings, i.e., lk(10,1) = −1.

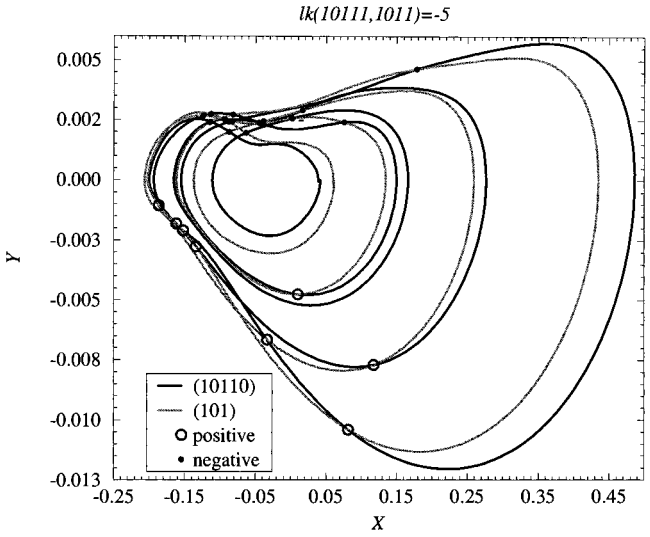

Figure 5. A couple of periodic orbits whose segments are close to tangency, implying spurious crossings.

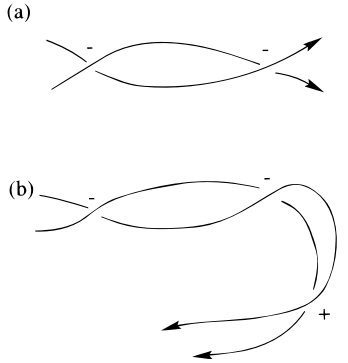

Figure 6. Examples of spurious crossings that are removed, being considered as artifacts. In (a), the relative positions of the two strands at the beginning and at the end of the small interval are the same and the crossings are not taken into account. Conversely, (b) corresponds to a situation where the relative positions of the two strands are different; one negative crossing is therefore counted, and the two close negative crossings are not considered as spurious.

since the relative positions of the two strands are the same. In the case of Figure 6b, the first two negative crossings are not considered as spurious, since the relative positions of two strands are reversed and, consequently, the second negative crossing is vanished by the positive crossing under an isotopy. This removal procedure has been introduced by Lefranc and Glorieux[22] and used by Boulant et al[23,24] on experimental data generated by a laser system. With this procedure, we find that all linking numbers may be predicted by a template defined by a linking matrix reading as

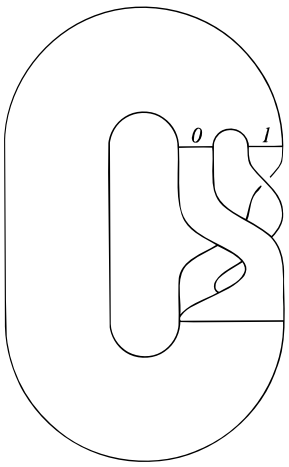

Figure 7. Template of the Belousov−Zhabotinskyi reaction extracted from the experimental data.

$$M_{ij} = \begin{bmatrix} 0 & -1 \\ -1 & -1 \end{bmatrix} \tag{3}$$

where M_{ii}'s are equal to the number of π-twists of the ith strip and off-diagonal elements M_{ij} ($i \neq j$) are given by the algebraic number of intersections between the ith and jth strips. The template associated with the linking matrix of relation 3 is displayed in Figure 7, accounting for the standard insertion convention,[25] which tells us that strips must be reinjected in the bottom band from back to front and from left to right. Explanatory details for such a topological characterization procedure are extensively discussed in refs 11, 19, and 20.

3. Topology of a Reconstructed Model

It has been demonstrated that a set of ordinary differential equations can be automatically reconstructed from a deterministic scalar time series (refs 12, 13, and 26−28 and references therein), a process that is called global vector field reconstruction leading to a model. As for a phase space reconstruction, the model may be equivalently reconstructed by using delay coordinates,[13,29] derivative coordinates,[12,26,27] or also principal components. Here, we use again derivative coordinates. Since the embedding dimension d_E is equal to 3; as for the BZ reaction, the global reconstructed model reads as

$$\begin{cases} \dot{X} = Y \\ \dot{Y} = Z \\ \dot{Z} = F_S(X,Y,Z) \end{cases} \tag{4}$$

where the dynamical variables are the successive derivatives

$$\begin{cases} X = x(t) = [Ce^{4+}(t)] \\ Y = \dot{x}(t) \\ Z = \ddot{x}(t) \end{cases} \tag{5}$$

The function F_S is written in the form

$$F_S = \sum_{i=1}^{N_p} K_p P^p \tag{6}$$

where $P^p = X^i Y^j Z^k$. The standard function F_S is approximated by using a multivariate polynomial basis on nets[27] which may be built by means of a Gram−Schmidt orthogonalization procedure.[30] The algorithm requires the definition of reconstruction parameters which are (i) the dimension d_E of the embedding space; (ii) N_q, the number of vectors on the net,

$$(X_{1,i}, X_{2,i}, ..., X_{d_E,i}, \dot{X}_{d_E,i}) \; (i \in [1, N_q])$$

with i a time index; (iii) N_s, the number of vectors sampled per pseudoperiod; (iv) N_p, the number of retained multivariate polynomials; (v) τ_w, the window size on which the derivatives are estimated by using a sixth degree interpolation polynomial. These interpolation polynomials are built, centered at each point, by using the six nearest neighbors. Derivatives are then obtained by analytically deriving these polynomials. The window size τ_w is taken to be equal to 7 times δt.

In practical applications, the choice of such parameters may have a significant effect on the quality of the results.[27] A guideline for choosing a generally good driving vector is based on an error function E_r according to

$$E_r = \frac{\sum_{i=1}^{N_q} |\dot{Z}_i - \tilde{F}_s(X_i, Y_i, Z_i)|}{\sum_{i=1}^{N_q} |\dot{Z}_i|} \tag{7}$$

This error function is calculated by using absolute values for computational efficiency.

E_r may be understood as a relative error between the value of the standard function directly evaluated from the time series and the one obtained from its approximation. For a given value of N_q, optimal values for N_s and the number of polynomials N_p are obtained by minimizing the error function. However, the value of N_q at which the minimized error funtion passes through a minimum or a local minimum does not warrant a correct integration. Therefore, the search of a successful global vector field reconstruction needs systematical trials.

In this case, excepted the measured variable X, which is here defined as $[Ce^{4+}(t)]$, the two other variables cannot be directly associated with any concentration since they are derivatives.

A good approximation $\tilde{F}_S$ of the function F_S is found with the following values of the reconstruction parameters:

$$\begin{cases} N_q = 650 \\ N_s = 12 \\ N_p = 56 \end{cases} \tag{8}$$

The reconstructed model is therefore found to be constituted by a standard function with 56 terms. By integrating this reconstructed model, whose coefficient spectrum $\{K_p\}$ is reported in Table 2, a plane projection of the chaotic attractor may be obtained as displayed in Figure 8, where experimental data are also superimposed. At first sight, experimental trajectory and integrated trajectory seem to be in a good agreement at least for low-amplitude oscillations (no large-amplitude oscillations are observed with this reconstructed model).

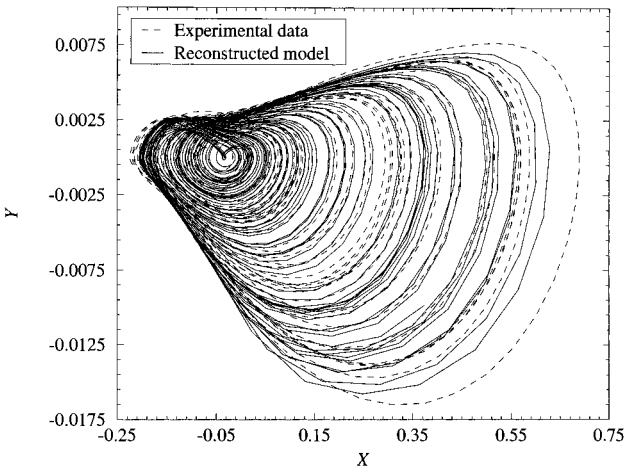

Figure 8. Phase space projection obtained by integrating the reconstructed model.

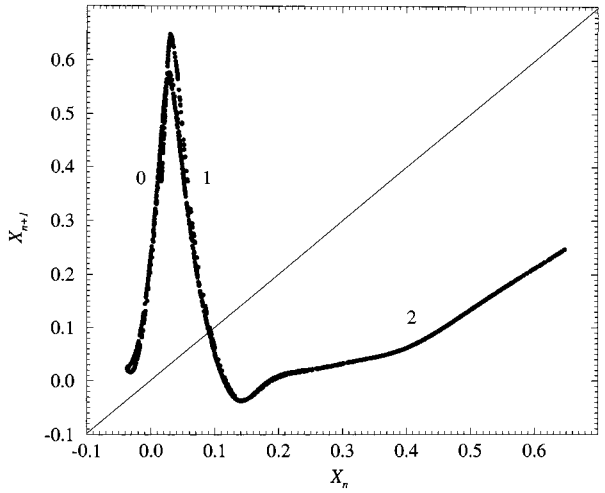

Figure 9. First-return map to a Poincar section for the reconstructed model.

Since it is possible to integrate the reconstructed model during a long time, we now possess a large amount of pseudoperiods, allowing an easy extraction of periodic orbits. The populations of extracted periodic are then reported in Table 3. By using a Poincaré section, a first-return map is computed and three monotonic branches are clearly evidenced (Figure 9), while the first-return map associated with the experimental data only exhibits two monotonic branches (Figure 3). The attractor generated by the reconstructed model may therefore be splitted into three strips whose topological properties are different (Figure 10).

By counting linking numbers between couples of periodic orbits (for instance, Figure 11), we found that the template characterizing the reconstructed model is as displayed in Figure 10. Its linking matrix reads as

$$M_{low} = \begin{bmatrix} 0 & -1 & -1 \\ -1 & -1 & 0 \\ -1 & 0 & 0 \end{bmatrix} \tag{9}$$

We then observed that all linking numbers between periodic orbits extracted from the experimental data are in agreement with the proposed template displayed in Figure 10. The template associated with the reconstructed model is therefore compatible with the one extracted from the data; that is, strips 0 and 1 are identical, and an additional strip is identified on the reconstructed template. Such a third strip cannot be exhibited from the data

TABLE 2: Coefficients of the Two Reconstructed Models[a]

p	i	j	k	Kp_A	Kp_B
1	0	0	0	$-1.708\,186\,975\,080\,1 \times 10^{-7}$	$1.171\,616\,357\,575\,4 \times 10^{-7}$
2	1	0	0	$-1.082\,449\,006\,678\,2 \times 10^{-5}$	0
3	0	1	0	$-6.649\,382\,802\,416\,2 \times 10^{-4}$	$-8.148\,626\,498\,228\,9 \times 10^{-4}$
4	0	0	1	$7.472\,649\,311\,745\,1 \times 10^{-3}$	$2.371\,674\,921\,655\,7 \times 10^{-2}$
5	2	0	0	$8.945\,164\,745\,971\,2 \times 10^{-5}$	$2.372\,138\,851\,847\,1 \times 10^{-4}$
6	1	1	0	$-7.716\,014\,511\,823\,1 \times 10^{-3}$	$-1.212\,971\,083\,614\,4 \times 10^{-2}$
7	1	0	1	0.432 078 094 205 03	0.796 721 690 105 41
8	0	2	0	0.274 789 719 635 90	0.224 915 341 828 76
9	0	1	1	−5.601 779 100 789 7	−9.947 458 573 077 4
10	0	0	2	234.881 794 063 83	409.808 771 359 58
11	3	0	0	$2.065\,777\,687\,221\,7 \times 10^{-3}$	$2.002\,252\,650\,014\,9 \times 10^{-3}$
12	2	1	0	−0.140 495 471 546 96	−0.166 622 228 663 9
13	2	0	1	3.374 238 156 624 2	2.671 892 422 783 4
14	1	2	0	1.798 602 796 778 0	0.638 662 330 491 95
15	1	1	1	−121.504 674 673 87	−180.702 746 366 15
16	1	0	2	−101.488 728 185 530	−1540.385 580 911 7
17	0	3	0	48.264 655 408 453	56.113 495 795 329
18	0	2	1	−3427.640 773 001 3	−5121.448 339 046 1
19	0	1	2	62458.490 201 442	42637.604 489 078
20	0	0	3	−2 326 623.539 428 7	−3646 013.173 390 1
21	4	0	0	$5.203\,716\,096\,025\,7 \times 10^{-3}$	$-8.201\,952\,915\,177\,4 \times 10^{-4}$
22	3	1	0	−0.539 605 583 988 72	−0.116 175 027 338 1
23	3	0	1	1.988 753 931 569 8	−16.714 678 223 064
24	2	2	0	−6.869 955 063 464 7	−7.084 784 111 920 9
25	2	1	1	50.910 979 461 748	1013.523 585 530 0
26	2	0	2	−9342.892 606 663 9	−26 713.218 192 470
27	1	3	0	677.350 657 280 34	811.396 858 541 84
28	1	2	1	6598.375 757 315 5	12773.974 485 589
29	1	1	2	641 073.354 476 63	1 199 836.568 426 2
30	1	0	3	−2 537 370.918 676 0	−3 620 760.529 813 7
31	0	4	0	992.541 145 877 01	4268.518 226 357 5
32	0	3	1	−280 511.515 085 74	−201 037.450 886 98
33	0	2	2	18 009 535.588 376	27 769 813.500 315
34	0	1	3	91 541 681.724 466	75 665 073.218 272
35	0	0	4	1134 214 625.8083	3 652 858 259.6129
36	5	0	0	$-7.153\,615\,662\,960\,6 \times 10^{-3}$	$-2.225\,152\,869\,472\,6 \times 10^{-2}$
37	4	1	0	0.120 299 671 304 51	2.114 487 908 692 2
38	4	0	1	−1.024 649 601 221 0	−35.242 597 786 874
39	3	2	0	37.036 366 775 158	7.315 786 068 703 4
40	3	1	1	−877.272 955 506 59	1845.787 009 850 3
41	3	0	2	13 733.712 371 085	−8184.962 321 0523
42	2	3	0	433.687 147 638 48	−2157.457 197 375 5
43	2	2	1	34 995.345 645 103	29 578.447 921 501
44	2	1	2	−410 624.975 269 34	−1 435 970.985 438 7
45	2	0	3	5 434 347.553 349 4	−9 991 649.531 581 2
46	1	4	0	−34 704.993 652 519	−24 239.582 282 112
47	1	3	1	−699 100.319 549 30	−1 485 240.178 739 5
48	1	2	2	586 736.444 632 55	12 411 611.651 104
49	1	1	3	478 828 413.089 73	−1 690 372 404.382 2
50	1	0	4	2 322 108 972.7087	−18 871 936 905.517
51	0	5	0	−914 180.792 998 57	−574 338.288 631 80
52	0	4	1	−58 290 300.849 396	−38 260 976.568 584
53	0	3	2	−954 968 572.374 42	508 357 655.862 26
54	0	2	3	−6 471 080 345.3770	−9 880 153 621.4250
55	0	1	4	68 494 316 256.813	−486 273 515 173.86
56	0	0	5	1 858 295 965 871.4	−6 966 010 723 383.8

[a] Kp_A for the low-amplitude model and Kp_B for the large-amplitude model.

TABLE 3: Population of Periodic Orbits Extracted from the Phase Portrait Generated by the Low-Amplitude Model

(1)	(210)	(2010)	(20021)	(20210)
(10)	(211)	(2021)	(20121)	(21210)
(20)	(1011)	(2110)	(20102)	(21100)
(21)	(2002)	(2111)	(20202)	
(101)	(2012)	(2101)	(20212)	
(201)	(2011)	(2100)	(20211)	

since the number of revolutions on the attractors is not sufficient. Indeed, the 4381 points used to compute the first-return map of the reconstructed model are more numerous than the 246 points used for the experimental data. The reconstructed model therefore allows one to exhibit the dynamical properties of the experiment, which are not necessarily identified on the experimental data.

4. Normal-Form Model

Arnodo et al[7] have studied the bifurcations underlying the abrupt transition to well-developed chaos in the BZ reaction. They identified this bifurcation as a subcritical Hopf bifurcation. Within the limits of experimental resolution of the control parameter φ, this subcritical Hopf bifurcation is indeed located in the vicinity of the homoclinic bifurcation associated with the spiraling behavior observed in the phase portrait.

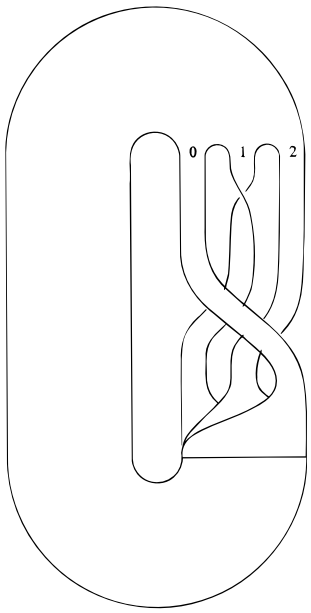

Figure 10. Template of phase portrait generated by the reconstructed model.

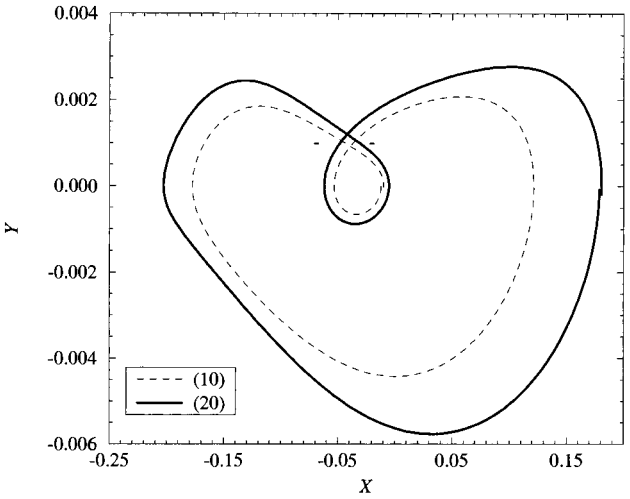

Figure 11. A couple of periodic orbits encoded by (20) and (10), respectively. The linking number lk(20,10) is found to be equal to −2.

Rather than using a reduction of the complex original chemical scheme, Arnodo et al[31] have derived a 3D model as the normal form of a triple instability. This normal form reads as

$$\begin{cases} \dot{X} = Y \\ \dot{Y} = Z \\ \dot{Z} = -\eta Z - \nu Y - \mu X - k_1 X^2 - k_2 Y^2 - \\ \qquad\qquad k_3 XY - k_4 XZ - k_5 X^2 Z \end{cases} \tag{10}$$

where control parameters are fixed as follows:

$$\begin{aligned} k_1 &= -1 & k_4 &= -0.2 \\ k_2 &= 1.425 & k_5 &= -0.01 \\ k_3 &= 0 & \eta &= 1 \end{aligned} \tag{11}$$

Control parameters μ and ν have a particular role later specified. This system accounts for the interaction of the Hopf bifurcation and of the homoclinic bifurcation previously mentioned. The

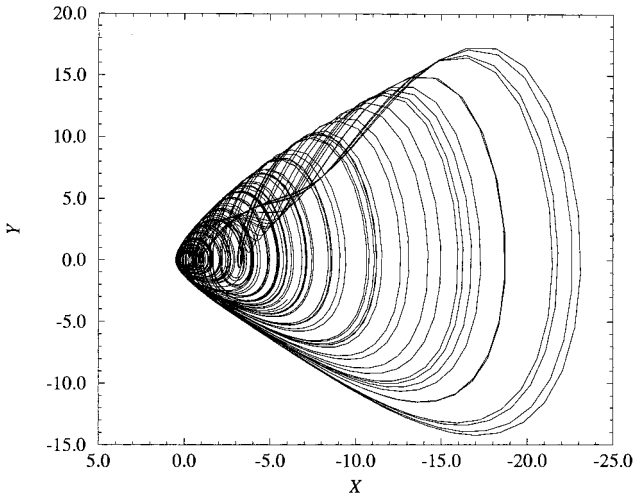

Figure 12. Phase space projection obtained by integrating the NF model.

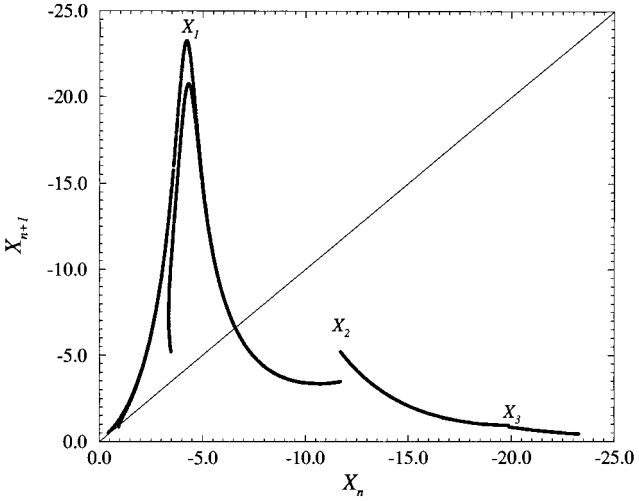

Figure 13. First-return map to a Poincaré section for the NF model.

model (10) has two fixed points

$$F_0 = \begin{vmatrix} 0 \\ 0 \\ 0 \end{vmatrix} \quad \text{and} \quad F_1 = \begin{vmatrix} -\dfrac{\mu}{k_1} \\ 0 \\ 0 \end{vmatrix} \tag{12}$$

In general, the origin displays a Hopf bifurcation when $\mu = \eta\nu$ (η, $\nu > 0$). For the chosen set of parameter values (in particular $\eta = 1$), the Hopf bifurcation at the origin is subcritical for $\mu = \nu > \nu^*$ with $\nu^* \approx 0.95$. The Hopf bifurcation appears for $\mu = 1.3$ and the homoclinic bifurcation for $\mu = 1.505$. The homoclinic orbit satisfies Sil'nikov's condition since

$$\begin{cases} -\lambda = -1.083 \\ \rho \pm i\omega = 0.041 \pm i1.178 \end{cases} \tag{13}$$

leading to a ratio of $\rho/\lambda \approx 0.038 \ll 1$.

A chaotic behavior is obtained for $\mu = 1.38$ and the corresponding attractor is displayed in Figure 12. A first-return map is computed (Figure 13). Three critical points are exhibited implying a generating partition defining four strips. Indeed, there is a discontinuity at X_3 since two strands of a chaotic trajectory that undergoes on the fourth strip present five negative crossings (Figure 14), while only three crossings are found between two strands undergoing on the third strip. The disconstinuity X_3

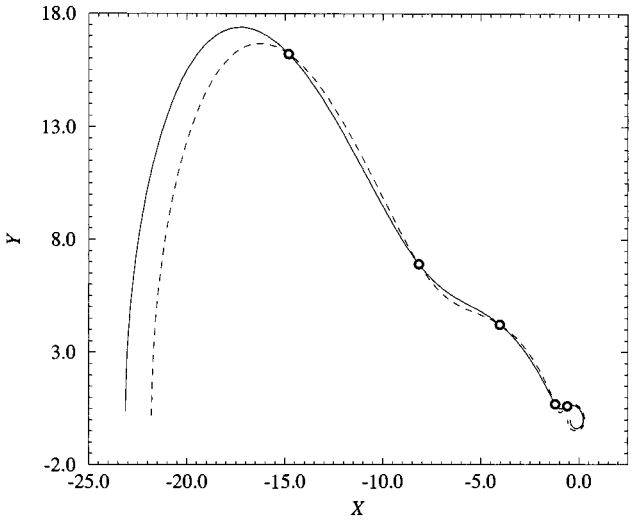

Figure 14. Two segments of the chaotic trajectory encoded by 5 according to the partition exhibited by the first-return map present five negative crossings, i.e., the strip 5 undergoes five negative half-turns.

TABLE 4: Linking Numbers Counted on Plane Projections of Periodic Orbits[a]

	(1)	(10)	(30)	(300)	(301)	(101)	(500000)
(10)	−1						
(30)	−1	−2					
(300)	−1	−2	−3				
(301)	−1	−2	−3	−4			
(101)	−1	−2	−3	−3	−3		
(500000)	−1	−2	−3	0	0	−3	
(500001)	−1	−2	−3	0	0	−3	0

[a] They are found to be equal to those predicted by the template defined by the linking matrix (7) except for five of them which are not retained due to the presence of segments close to tangency. Note that, in this population, the symbol "5" only appears in period-6 orbits.

therefore separates the third and the fourth strips. Periodic orbits are then extracted up to period-6 included and encoded as follows:

$$\sigma_n = \begin{cases} 0 & \text{if } X_n > X_1 = -4.26 \\ 1 & \text{if } X_1 > X_n > X_2 = -11.74 \\ 3 & \text{if } X_2 > X_n > X_3 = -19.88 \\ 5 & \text{if } X_3 > X_n \end{cases} \tag{14}$$

The parity of symbols are fixed to associate an even integer with an increasing branch and an odd integer with a decreasing branch. A certain set of linking numbers (reported in Table 4) has been computed and found to be well predicted by a template whose linking matrix reads as

$$M_{\mathrm{NF}} = \begin{bmatrix} 0 & -1 & -1 & -1 \\ -1 & -1 & -2 & -2 \\ -1 & -2 & -3 & -4 \\ -1 & -2 & -4 & -5 \end{bmatrix} \tag{15}$$

The template is displayed Figure 15. It is found to be compatible with the one extracted from the experimental data since strips 0 and 1 are linked in the same way. Nevertheless, even if the model exhibits the same sequence of bifurcations implying the fixed points, the phase portrait generated by the NF model seems to be rather different than the one for the dynamics underlying the experimental data. This may be easily seen by comparing the plane projection of the phase portrait for the reconstructed

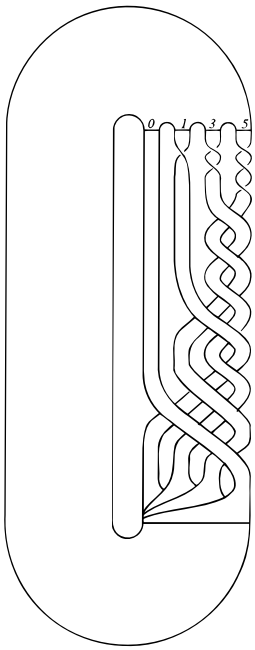

Figure 15. Template of the NF model.

data (Figure 2) and the plane projection of the attractor generated by integrating the normal-form model (Figure 12). Also, more precisely, the experimental dynamics generates a two-strip template (two monotonic branches in the first-return map), in contrast with the NF model that generates a four-strip template. Moreover, the reconstructed model, which accurately reproduces the dynamics of the experimental data is found to be characterized by a template that is not compatible with the template extracted from the attractor generated by the NF model. The NF model does not therefore provide an adequate model to describe the dynamics of the experiment. It is then rejected for the reconstructed model.

5. Conclusion

The Belousov−Zhabotinskyi reaction is governed by a very complex chemical kinetics, implying at least 20 species. A reduced dynamics has been found to be described by a set of seven ordinary differential equations. Nevertheless, it has been shown that the asymptotic chaotic behavior may be embedded in a 3D space and described by a set of three ordinary differential equations. This reconstructed model has been validated by a topological characterization in which the topological organization of periodic orbits is synthesized in an object called a reconstructed template. Indeed, the template generated by the model is compatible with a template directly extracted from experimental data. These templates are however not compatible with the template of a so-called NF model. Although the NF model succeeds in reproducing some important features of the BZ reaction, it is, however, invalidated by its failure of reproducing the topological organization of the data. An advantage of the global vector field reconstruction technique lies in its ability to directly generate models from experimental data, without any prior knowledge of the mechanisms underlying the dynamics. This technique has been here applied to the reduction of a complex chemical kinetics. Also, as a result of its ability to remove some amount of noise contamination, the technique allows one to exhibit and characterize fine structures hidden in the experimental data. The success of the technique also provides strong evidence for the existence of deterministic chaos in the BZ reaction, in a way not explored up to now.

Furthermore, a dynamics more complex than a trivial horseshoe dynamics has been exhibited.

References and Notes

(1) Zhabotinskii, M. A. *Biofizika* **1964**, *9*, 306.
(2) Field, J. R.; Körös, E.; Noyes, R. M. *J. Am. Chem. Soc.* **1972**, *94* (25), 8649.
(3) Belousov, B. P. A periodic reaction and its mechanism. *Sbornik Referatov po Radiatsionni Meditsine*; Medgiz: Moscou, 1958; p 145.
(4) Schmitz, R. R.; Graziani, K. R.; Hudson, J. L. *J. Chem. Phys.* **1977**, *67*, 3040.
(5) Edelson, D.; Field, R. J.; Noyes, R. M. *Int. J. Chem. Kinet.* **1975**, *7*, 417.
(6) Richetti, P.; Arnodo, A. *Phys. Lett. A* **1985**, *109* (8), 359.
(7) Arnéodo, A.; Argoul, F.; Elezgaray, J.; Richetti, P. *Physica D* **1993**, *62*, 134.
(8) Argoul, F.; Arnéodo, A.; Richetti, P.; Roux, J. C.; Swinney, H. L. *Acc. Chem. Res.* **1987**, *20*, 436.
(9) Roux, J. C.; Simoyi, R. H.; Swinney, H. L. *Physica D* **1983**, *8*, 257.
(10) Richetti, P.; De Kepper, P.; Roux, J. C.; Swinney, H. L. *J. Stat. Phys.* **1987**, *48* (5/6), 977.
(11) Mindlin, G. B.; Solari, H. G.; Natiello, M. A.; Gilmore, R.; Hou, X. J. *J. Nonlin. Sci.* **1991**, *1*, 147.
(12) Letellier, C.; Le Sceller, L.; Dutertre, P.; Gouesbet, G.; Fei, Z.; Hudson, J. L. *J. Phys. Chem.* **1995**, *99*, 7016.
(13) Brown, R.; Rul'kov, N. F.; Tracy, E. R. *Phys. Lett. A* **1994**, *194*, 71.
(14) Letellier, C.; Gouesbet, G.; Rulkov, N. *Int. J. Bif. Chaos* **1996**, *6* (12B), 2531.
(15) Takens, F. Detecting Strange Attractors in Turbulence. In *Dynamical Systems and Turbulence, Warwick 1980*; Lecture Notes in Mathematics 898; Rand, D. A., Young, L. S., Eds.; Springer-Verlag: New York, 1981; pp 366−381.
(16) Broomhead, D. S.; King, G. P. *Physica D* **1986**, *20*, 217.
(17) Gibson, J. F.; Farmer, J. D.; Casdagli, M.; Eubank, S. *Physica D* **1992**, *57*, 1.
(18) Argoul, F.; Arnéodo, A.; Richetti, P. *Phys. Lett. A* **1987**, *120* (6), 269.
(19) Tufillaro, N. B.; Abbott, T.; Reilly, J. *An Experimental Approach to Nonlinear Dynamics and Chaos*; Addison-Wesley: New York, 1992.
(20) Letellier, C.; Dutertre, P.; Maheu, B. *Chaos* **1995**, *5* (1), 271.
(21) Mindlin, G. B.; Hou, X. J.; Solari, H. G.; Gilmore, R.; Tufillaro, N. B. *Phys. Rev. Lett.* **1990**, *64* (20), 2350.
(22) Lefranc, M.; Glorieux. P. *Int. J. Bif. Chaos* **1993**, *3* (3), 643−650.
(23) Boulant, G.; Lefranc, M.; Bielawski S.; Derozier, D. *Phys. Rev. E* **1997**, *55* (5), 5082−5091.
(24) Boulant, G.; Lefranc, M.; Bielawski S.; Derozier, D. *Int. J. Bif. Chaos*, in press.
(25) Melvin, P.; Tufillaro, N. B. *Phys. Rev. A* **1991**, *44* (6), 3419.
(26) Gouesbet, G.; Maquet, J. *Physica D* **1992**, *58*, 202.
(27) Gouesbet, G.; Letellier, C. *Phys. Rev. E* **1994**, *49* (6), 4955.
(28) Tufillaro, N. B.; Wyckoff, P.; Brown, R.; Schreiber, T.; Molteno, T. *Phys. Rev. E* **1995**, *51* (1), 164.
(29) Serre, T.; Kolláth, Z.; Buchler, J. R. *Astron. Astrophys.* **1996**, *311*, 833.
(30) Letellier, C.; Ringuet, E.; Maheu, B.; Maquet, J.; Gouesbet, G. *Entropie* **1997**, *202*/*203*, 147.
(31) Arnodo, A.; Spiegel, E. A.; Tresser, C. *Physica D* **1985**, *14*, 327.